DOI: 10.1002/cphc.200800099

Self-Assembled Au Nanoparticles as Substrates for Surface-Enhanced Vibrational Spectroscopy: Optimization and Electrochemical Stability

Meikun Fan and Alexandre G. Brolo*[a]

Three-dimensional nanostructured metallic substrates for enhanced vibrational spectroscopy are fabricated by self-assembly. Nanostructures consisting of one to 20 depositions of 13 nm-diameter Au nanoparticles (NPs) on Au films are prepared and characterized by means of AFM and UV/Vis reflection–absorption spectroscopy. Surface-enhanced polarization modulation infrared reflection–absorption spectroscopy (PM-IRRAS) is observed from Au NPs modified by the probe molecule 4-hydroxythiophenol. The limitation of this kind of substrate for surface-enhanced PM-IRRAS is discussed. The surface-enhanced Raman scattering (SERS) from the same probe molecule is also observed and the effect of the number of Au-NP depositions on the SERS efficiency is studied. The SERS signal from the probe molecule maximizes after 11 Au-NP depositions, and the absolute SERS intensities from different batches are reproducible within 20%. In situ electrochemical SERS measurements show that these substrates are stable within the potential window between −800 and +200 mV (vs. Ag/AgCl/sat. Cl^-).

Introduction

The analytical spectroscopic signal from species adsorbed on metallic nanostructures can be significantly enhanced relative to the signal from the same species in solution;[1,2] for instance, surface-enhanced Raman scattering (SERS) as high as 10^{14}–10^{15} times the normal Raman response has been reported for species located at the "hot spots" of nanostructured silver.[3] SERS and surface-enhanced infrared spectroscopy (SEIRS) are vibrational spectroscopy tools and the uniqueness of the vibrational signature makes it possible to identify target molecules.[2] The SERS technique is particularly attractive for label-free trace analysis, such as the detection of high explosives, nerve stimulants, and environmental pollutants.[4]

It is currently widely accepted that there are mainly two kinds of contributions to the observed SERS[1,4,5] and SEIRS:[6,7] the charge-transfer (CT) mechanism and the electromagnetic (EM) mechanism. The CT mechanism originates from resonant transitions involving the metal's Fermi level and the adsorbed molecule's frontier orbitals.[5,8] In an electrochemical environment, this contribution can be tuned by adjusting the applied potential.[5] The CT is thought to be a short-range effect, which affects mainly the species in direct contact with the metal surface. Localized surface plasmons (LSPs) can be directly excited on nanostructured noble-metal surfaces by using visible radiation, and these resonances are considered to provide the main contributions to the EM mechanism.[5–8] LSPs result in strong EM fields localized in certain regions of the nanostructured surface (for example, sharp tips and troughs between nanoprotrusions[9]), which account for most of the observed enhancement. The frequency of the LSP resonance is tunable by the surface morphology.[10–18]

A variety of substrates that support SERS are being explored by various groups.[1,4,19] Typically, an ideal SERS substrate for analytical applications should be robust, easy to prepare and use, provide a large enhancement of the interference-free Raman signal of the analyte, and present a high degree of reproducibility.[4] Substrate development is also a highly active area in SEIRS research. The substrates developed specifically for SEIRS include vacuum-deposited metal islands,[6] nanorod arrays,[20] subwavelength holes,[21] and nanoparticles (NPs).[6,7,22–27] Recently, a SEIRS enhancement factor of 2000 was achieved by "in situ" tailoring of the size of the metallic nanofeatures.[24]

Metallic NPs are probably the most common type of substrate for SERS and SEIRS. They are easy to prepare (with numerous choices of sizes and shapes, which means tunable LSPs), and can be simply characterized by UV/Vis spectroscopy. Metallic NPs aggregate in the presence of salts, thus leading to a large enhancement factor.[4] However, the morphology of the aggregates and the reproducibility of the enhanced signal[19] are strongly affected by the experimental conditions, such as temperature, ionic strength, pH, and even the presence of adsorbates.[4]

Gold and silver NPs can be self-assembled into mono- or multilayer 3D structures on a flat surface.[15,28] This kind of approach for SERS-substrate preparation has recently attracted much attention.[11,28–34] The self-assembled structures are fabricated by alternately dipping the initially flat surface into solutions containing a bifunctional cross-linker and the NPs. The resultant morphology can be tuned by the desired number of NP depositions, which tailors the substrate performance for SERS. The sizes of the linker molecules and of the NPs are adjustable, thus providing more dimensions to tune the resonan-

[a] *M. Fan, Dr. A. G. Brolo*
Department of Chemistry, University of Victoria
Victoria, BC, V8W 3V6 (Canada)
Fax: (+1) 250-7217147
E-mail: agbrolo@uvic.ca

ces. It has also been shown that it is possible to use this approach to fabricate a specific substrate that matches the excitation condition (laser wavelength) of the SERS experiment, which leads to optimized enhancement conditions.[29] However, the self-assembled nanostructure multilayer approach described above has not yet been explored to develop substrates for SEIRS.

Metallic-NP-modified electrodes also provide advantages over the traditional "bulk" electrodes used in electrochemistry;[35–37] for example, NPs usually demonstrate extra catalytic activities, even for those metals normally recognized as inert, such as Au.[37] Furthermore, NP-modified electrodes can provide higher signal-to-noise ratios for electrochemical current measurements as a result of their large effective surface area.[36] In fact, theoretical calculations reveal that an electrode composed of 10 nm NPs in an array format can enhance the peak current by two orders of magnitude compared to a bulk electrode.[35]

All these advantages have attracted several groups to the development of metallic-NP-modified electrodes for both electrocatalysis and in situ SERS.[14,38–40] These activities have even expanded towards nontraditional SERS-active metals; for instance, Gomez et al.[14] reported that Pt NPs deposited on a flat conducting electrode surface provided a significantly larger SERS enhancement factor than an electrochemically roughened Pt electrode. Guo et al.[40] found that 3 nm Fe NPs made by microemulsion also demonstrated remarkable SERS activity when coated onto a flat silver electrode. Potential-dependent SERS spectra of pyridine were recorded from the Fe NPs with an enhancement factor of two to three orders of magnitude.[40] Despite all this activity in the field, there is no report yet on the application of 3D self-assembly using more common NPs, such as gold, for surface enhancement on smooth electrode surfaces for SEIRS and for in situ electrochemical SERS applications. These structures should provide high SERS signal enhancement,[29,30] as well as the good electrical conductivity required for electrocatalysis.[28,33,34]

Previously, we demonstrated that the stepwise deposition of Au NPs on glass produced a highly sensitive SERS substrate.[29] It was found that under optimum conditions, the SERS intensity could be at least ten times stronger than that of a monolayer of Au NPs. More importantly, by changing the number of depositions we were able to tune the surface morphology to match the laser wavelength, thus producing an optimized SERS substrate for a given condition for surface-plasmon (SP) excitation. In the work reported herein, we fabricated similar structures on a thin gold film instead. The conditions for optimum surface-enhanced vibrational spectroscopy were evaluated and the performance of the substrate for in situ electrochemical SERS measurements was probed.

Results and Discussion

Characterization of the Substrates by AFM and UV/Vis Reflection–Absorption Spectroscopy

Figure 1 presents selected atomic force microscopy (AFM) images of substrates prepared with different numbers of Au-NP deposition steps. The AFM images indicate that both the surface roughness and the average size of the features increase with increasing number of depositions. The size of the features after one Au-NP deposition is around 10 nm (see Figure 1a), which is consistent with the diameter of the NPs used. Figure 1b shows that a large number of aggregates is formed after nine NP depositions. In this case, the average height is about 50 nm, but features as large as 100 nm can be found when a large area of the substrate ($100\times100\ \mu m^2$) is imaged (data not shown).

Figure 2 shows the UV/Vis reflection–absorption spectra from substrates with different numbers of Au-NP deposition steps. The UV/Vis spectrum after one Au-NP deposition presents an absorption maximum at around 524 nm, which is very close to that observed from the NPs in water (520 nm). The small red shift relative to the absorption of Au NPs in water and the peak width suggest a small degree of aggregation for the monolayer of immobilized NPs, in agreement with the AFM data from Figure 1. The 524 nm peak broadens and shifts to a longer wavelength as the number of Au-NP depositions

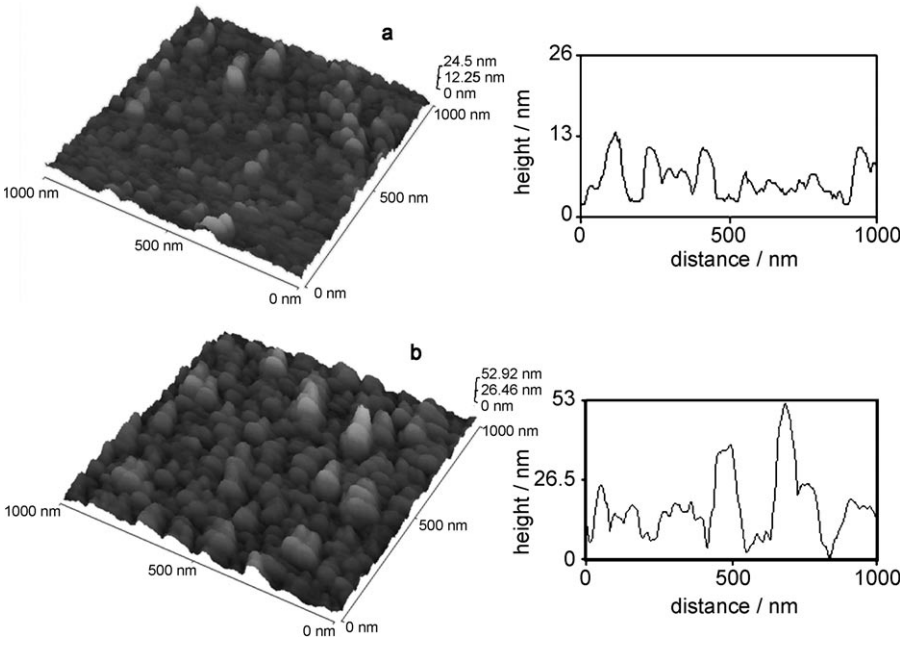

Figure 1. Topographic and representative line-scan AFM images of the Au-NP-modified substrates: a) one Au-NP deposition; b) nine Au-NP depositions.

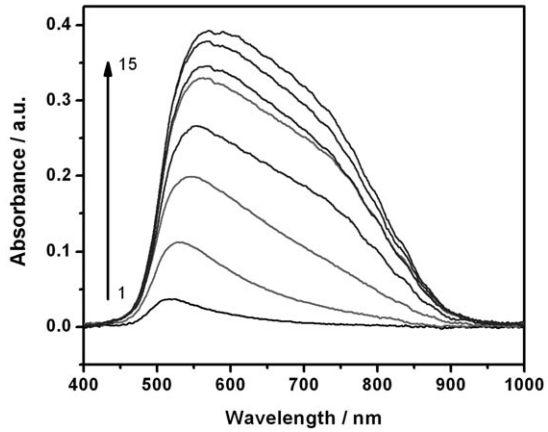

Figure 2. UV/Vis reflection–absorption spectra for substrates with different numbers of Au-NP depositions on Au slides. The spectra were calculated using: absorbance $= -\log(R_{NP}/R_{bareAu})$, where R_{NP} is the reflectivity from the Au slide modified with Au NPs (the average from different positions on the same slide is presented), and R_{bareAu} is the reflectivity from the Au slide without Au NPs. The detection system was equipped with a filter with cutoff at 450 nm.

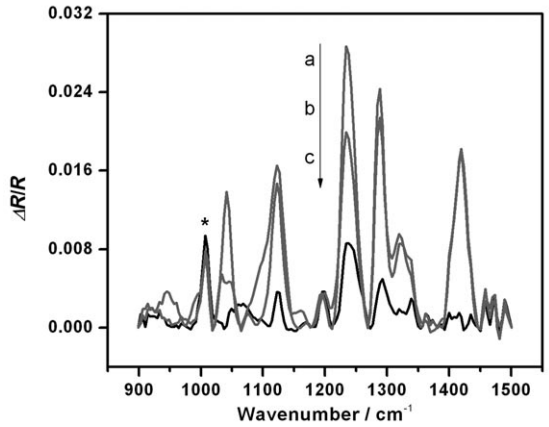

Figure 3. Polarization modulation infrared reflection–absorption spectra: a) one deposition of Au NPs; b) two depositions of Au NPs; c) zero deposition of Au NPs, that is, a monolayer of PDT on a flat gold substrate. All spectra were background-corrected. The peak at 1008 cm^{-1} (marked with an asterisk) is an artifact from the instrument. Also note that the amount of adsorbed PDT in (a) and (c) is the same, and is smaller than the amount of PDT adsorbed in (b) (see text and Scheme 1). *R*: reflectivity.

increases. A similar trend is observed for Au NPs deposited on glass.[29] These changes are accompanied by an increase in absorption in the region between 600 and 800 nm. All these findings are evidence of increasing aggregation with the number of Au-NP depositions. The total absorbance—given by the integrated area of the absorption spectrum—also increases. However, the changes are not as pronounced after nine Au-NP depositions, which is similar to our previous observations.[29]

A comparison between the results presented in Figure 2 (for Au NPs deposited on Au films) with our previous results (for Au NPs deposited on glass[29]) shows a few differences in the shape of the absorption profiles and their evolution with the number of Au-NP depositions. These differences can be attributed to the differences in the experimental procedures, surface chemistry, and optical properties of the underlying substrate (glass versus gold film).

Application of the Substrates to Enhanced Vibrational Spectroscopy

Substrate Optimization and Application in Surface-Enhanced PM-IRRAS

Representative spectra from polarization modulation infrared reflection–absorption spectroscopy (PM-IRRAS) of the Au-NP assemblies are shown in Figure 3, and they contain several vibrational features that can be readily assigned to the linker molecule (1,3-propanedithiol, PDT) used to immobilize the Au NPs on the gold electrode (see Scheme 1). The main vibrational bands in Figure 3 at 1419, 1323, 1288, and 1234 cm^{-1} have been previously assigned to the CH_2 bending/scissoring, CH_2 wagging, CH_2 twisting, and CH_2 twisting/wagging modes of PDT, respectively.[41] The complete assignment has been confirmed by our own ab initio calculation (DFT RB3LYP/6-311^{++}g(3df,3pd)). It should be pointed out that PDT presents three conformers, and the dom-

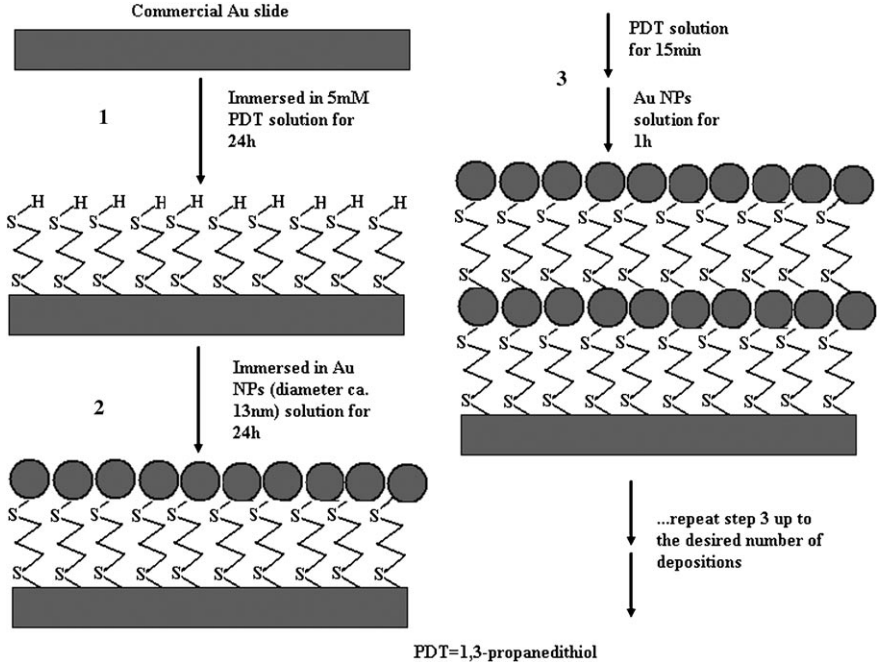

Scheme 1. Schematic representation of the procedure for deposition of Au NPs on a gold thin film. This diagram is not to scale. Notice that the amount of PDT before and after step 2 is the same.

inant conformation of the adsorbed molecule may be different from PDT in solution.[41,42]

In Figure 3, spectrum c with zero Au-NP depositions corresponds to the flat gold surface modified with a monolayer of PDT (in the absence of NPs). In this case, the IR features are weak and the band due to the CH_2 bending mode ($\approx$1419 cm^{-1}) is missing. The lack of a band due to CH_2 bending is an indication that only one thiol end of the PDT is directly adsorbed onto the gold surface, as pointed out by Joo et al.[42] When only one of the thiols of the PDT binds to the surface, which leaves the main chain almost perpendicular to the gold surface, the changes in dipole momentum due to CH_2 bending are parallel to the surface. According to the surface selection rules, only vibrational modes with transition dipole components perpendicular to the metallic surface contribute to the IR intensity.[43] Hence, this result indicates that an organized self-assembled monolayer (SAM) of PDT is formed.

Figure 3 also shows a significant increase in the IR absorption after the PDT monolayer is covered with a layer of Au NPs. Notice that the amount of PDT on a flat Au surface (a monolayer) is the same before and after deposition of the Au NPs (because the Au NPs are deposited on top of the PDT monolayer, see Scheme 1). However, the IR intensity of the latter is about four times larger at about 1234 cm^{-1} (Figure 3). It is well known that Au NPs can be used as a substrate for SEIRS measurements.[24–26,44] Therefore, the increase in the IR absorption relative to the smooth surface is attributed to the SEIRS effect. However, as can be seen in Figure 3, the IR absorption at approximately 1234 cm^{-1} actually decreases with additional NP-deposition steps (although after the first layer of Au NPs, the amount of PDT increases with the number of Au NP depositions, see Scheme 1).

This effect is better illustrated in Figure 4, which shows the dependence of the IR absorption of all PDT bands in the 1000 to 1500 cm^{-1} region versus the number of Au-NP depositions. It is clear that after five Au-NP depositions, the intensities of the different bands are comparable to those observed from a smooth gold surface modified with a PDT monolayer. These observations can be rationalized by considering the operation

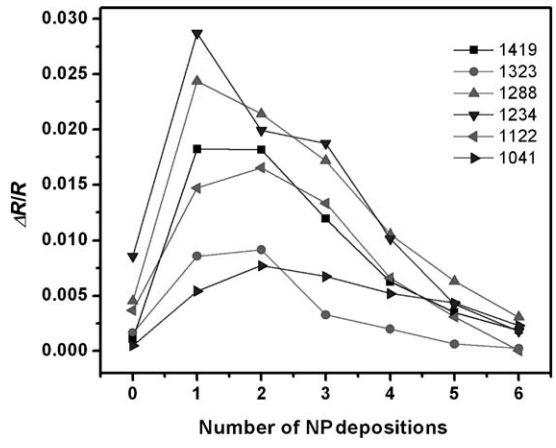

Figure 4. Dependence of the surface IR intensities of PDT bands on the number of Au-NP depositions.

principle of the PM-IRRAS technique. In PM-IRRAS, the incident light is modulated between p and s linear polarizations and the surface is probed by reflection. According to the surface selection rules for IR spectroscopy in external reflection configuration, the s polarization is not absorbed by the surface species on a highly reflective metal, whereas p-polarized incident light is absorbed. Therefore, the difference between the IR reflection and absorption from both polarizations eliminates the background, thus providing an IR absorption related only to the surface species. However, as the number of Au-NP depositions increases, the substrate surface becomes rougher. Rough structures are depolarizing (i.e., have a tendency to scramble polarized fields)[45,46] and in turn decrease the response towards the difference between s- and p-polarized incident light.

Figures 3 and 4 show that the maximum surface-enhanced PM-IRRAS for this class of substrates (Au NPs immobilized on a flat gold film using a dithiol linker) is obtained within the first few layers of deposited Au NPs. The relative intensities of the IR absorption bands also change with the number of Au-NP depositions; for instance, the 1234 cm^{-1} band is almost twice as large as the 1122 cm^{-1} band after the deposition of a monolayer of Au NPs; however, the ratio between these two bands is closer to one after two Au-NP depositions (Figure 3). These changes in relative intensities are explained by considering the average orientation of PDT. After adsorption, the PDT species covering the NPs are oriented randomly relative to the underlying gold surface. Therefore, the changes in relative intensities can be attributed to an increased distribution of orientations of PDT with the addition of Au NPs. Notice that the amount of adsorbed PDT increases linearly after the deposition of the second layer of Au NPs (see Scheme 1)

By considering the results from Figures 3 and 4, we concluded that the substrate prepared with just one Au-NP deposition step yielded a reasonable enhancement and decided to use it for the surface-enhanced IR absorption investigation of a probe molecule (4-hydroxythiophenol, 4-HTP). Moreover, since the PDT links the Au NPs to the Au surface, the remaining area of the NPs not in contact with the surface is free of PDT and may readily interact with the probe molecule (see Scheme 1) when the substrate with just one NP deposition is used.

Figure 5a shows the surface-enhanced IR spectrum of 4-HTP adsorbed on the optimized substrate. The spectra of a monolayer of 4-HTP adsorbed on a smooth Au surface (Figure 5b) and of the substrate in the absence of 4-HTP (Figure 5c) are also shown. A comparison between Figures 5a and 5b shows that the vibrational bands of the probe molecule are enhanced in the presence of Au NPs. It is believed that an increase in surface area can also contribute to the observed SEIRS signal.[6] Using AFM, it is found that the surface area after one Au-NP deposition is typically less than 1.2 times the value for the smooth gold surface. Electrochemical measurements obtained with a reversible redox pair ($[Fe(CN)_6]^{3-}$/$[Fe(CN)_6]^{4-}$) do not show an increase in the electrochemical surface area after the first Au-NP deposition (data not shown). These findings are consistent with the results reported by Sivanesan et al.,[47] where a similar electrochemical experiment was performed for the self-assembly of Au NPs on a SAM of 1,6-hexanedithiol.

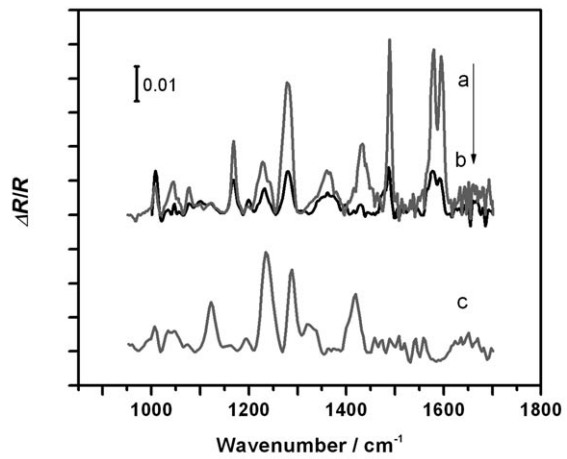

Figure 5. Polarization modulation infrared reflection–absorption spectra of a) 4-HTP on a slide modified by one deposition of Au NPs; b) 4-HTP on a bare Au slide; and c) a slide modified by one deposition of Au NPs in the absence of 4-HTP (SERS signal from the PDT). All spectra are background-corrected.

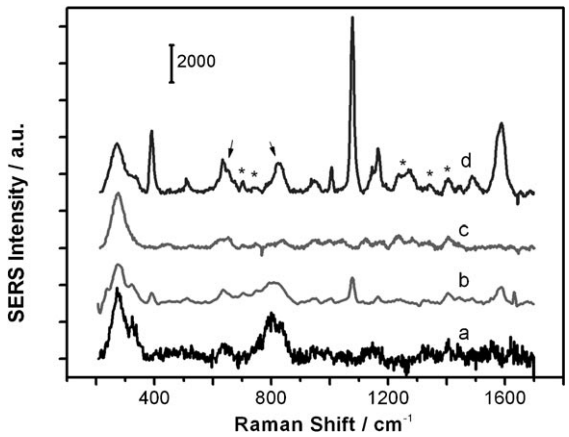

Figure 6. SERS spectra from substrates modified with Au NPs in the absence and presence of 4-HTP. Spectra from a) one deposition of Au NPs (without 4-HTP); b) 4-HTP adsorbed on one deposition of Au NPs; c) nine depositions of Au NPs (without 4-HTP); d) 4-HTP adsorbed on nine depositions of Au NPs. Spectra a and b are multiplied by a factor of ten. All spectra are baseline-corrected and are an average of four measurements on different regions of the same slide. The asterisks indicate the PDT bands and the arrows indicate bands with contributions from both PDT and 4-HTP.

Meanwhile, the enhancement factor for 4-HTP (which is of about four relative to the smooth surface) is about the same as that of PDT, for which the role of the surface area is absent, since the amount of PDT does not change after NP deposition. Thus, the increase in IR absorption for 4-HTP adsorbed on Au NPs (Figure 5 a) relative to 4-HTP adsorbed on the smooth surface (Figure 5 b) is assigned mainly to a surface-enhancement effect. On the other hand, we should point out that the surface-enhancement factor observed here (about four) is smaller than the values reported by other authors.[6,24]

It can also be seen in Figure 5 that absorptions from the linker PDT (shown in Figure 5 c) interfere with the final spectrum of 4-HTP on the Au-NP-modified substrate, since PDT and 4-HTP both have absorption bands around 1230, 1280, and 1420 cm^{-1}. In conclusion, although some vibrational bands from 4-HTP can be uniquely assigned, the interference from the linker is significant in this particular case. This problem severely limits the applicability of self-assembled Au NPs using linkers in surface-enhanced IR spectroscopy. Moreover, the enhancement factor obtained by this substrate is only at the lower end of that reported by other groups.[6] Therefore, different approaches for Au-NP immobilization, which do not include organic linkers, seem to be more suitable for SEIRS.[24–26]

Substrate Optimization for SERS

The compound 4-HTP was also used as a probe to evaluate the SERS efficiency of the substrates. Figure 6 shows the SERS spectra of substrates prepared with different numbers of Au-NP depositions with and without the SERS probe (4-HTP). The spectra in Figure 6 are baseline-corrected for a fluorescence-like background[48] that was observed in all experiments. This background increased with the deposition of NPs. The main features in the SERS of 4-HTP agree well with the report by Lee et al.[49] There are two important points that can be observed from Figure 6. Firstly, the SERS bands due to the linker (PDT) are present even in the absence of 4-HTP. This SERS background, however, is much weaker than the signal from the probe molecule. The SERS bands of PDT can be readily identified as weak features in the SERS spectra containing 4-HTP, as illustrated in Figure 6 d. Secondly, the magnitude of the SERS signal (from both the background linker and the probe) increase with the number of Au-NP depositions.

This trend is further illustrated in Figure 7, which shows a plot of the SERS signal from the ring breathing mode of 4-HTP against the number of Au-NP depositions. The SERS intensity increases with the number of NP depositions, thereby reaching a maximum value at around 11 Au-NP depositions. The results from Figure 7 are not corrected for surface-area variations. This procedure is justified by our surface-area determinations with two independent techniques, namely, AFM and electrochemistry. AFM shows an average increase in surface area of 20–30 %,

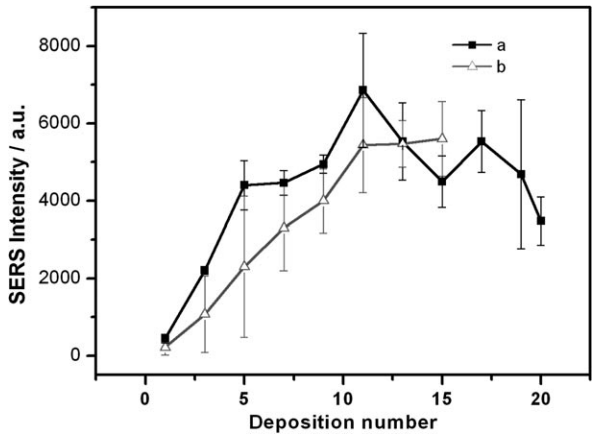

Figure 7. SERS intensity of the 4-HTP band at 1078 cm^{-1} versus the number of Au-NP depositions: a) Averages from a single-batch preparation; error bars: the results of four measurements on the same slide (different spots). b) Averages from three different batch preparations.

relative to the smooth surface, only after nine Au-NP depositions. The relatively small increase in surface area with the number of Au-NP depositions is consistent with our previous work.[50] The 20% variation in the electrochemical surface area is actually within the uncertainty of the SERS measurement.[51] Hu et al.[13] and Yun et al.[52] also reported the dependence of SERS intensity on the morphology of the metallic nanostructure, without taking into consideration the surface area, which was also assumed to have a minor effect compared to the SP contribution to the enhancement of the Raman signal.[53]

Previously, we investigated the relationship between the SERS signal and the number of Au-NP depositions on a glass substrate.[29] We found that the maximum SERS signal was dependent on the excitation wavelength, since different conditions for optimized SP resonance were encountered for distinct morphologies. An optimized SERS substrate for 632.8 nm excitation (He–Ne) was found after nine Au-NP depositions on glass.[29] On the other hand, the maximum in Figure 7 occurred after 11 Au-NP depositions; the SERS signal decreased by roughly 30% and remained stable (within the uncertainty of the SERS measurements) after the maximum. We attribute the discrepancy with our previous report to the differences in EM field distribution around the nanofeatures for Au NPs deposited on either glass or a flat gold film. These may include further contributions from additional plasmon hybridization, which is expected from the interaction between the metallic NPs with the metallic film.[54] Another factor is the structure of the linker used to build the first layer of Au NPs. When a gold film is used, the Au NPs are deposited on a monolayer of PDT. On the other hand, the glass surface was modified by 3-(mercaptopropyl)trimethoxysilane to allow the binding with Au NPs. Comparing the AFM results from Figure 1 with our former report,[29] it is found that although the heights of the features are similar for the same number of Au-NP depositions, the line scan shows that the features for Au NPs deposited on glass slides are somehow sharper, and the bumps are more isolated. These factors should significantly alter the conditions for SP excitation in these substrates, thus leading to differences in the trends for the number of Au-NP depositions.

The two curves in Figure 7 are for averages calculated from SERS measurements realized in different spots of the same slides (Figure 7a) and averages obtained from three different batches (Figure 7b). The calculated percent relative standard deviation (RSD%) of the SERS intensities measured at different positions on a single slide ranges from 20 to 40%, which is within the normal spatial variability encountered in conventional random SERS substrates.[51] The spatial variability, measured as RSD%, decreases with increasing number of Au-NP depositions. Furthermore, the variability of the SERS signal among batches (RSD%) is less than 20% after nine Au-NP depositions. These results imply that the variability in the SERS signal (both the spatial variability within a slide and the sample-to-sample variability) are within 20% after nine Au-NP depositions; in other words, the variability of the SERS signal decreases with the number of NP depositions. This is an important finding, since the reproducibility of the SERS signal is generally a concern that precludes the widespread application of the SERS technique in analytical problems. Another important aspect investigated is the long-term stability of the substrates. No deterioration in the SERS performance is found, even for three-month-old substrates that were stored in the dark.

Application of the Substrates for In Situ Electrochemical SERS

Another objective of this work is to use this class of substrates for in situ electrochemical SERS measurements. The Au NPs are immobilized by using a thiol linker. The Au–S bonds can be electrochemically dissociated; therefore, the electrochemical stability of the substrate needs to be evaluated prior to the introduction of a SERS probe. Moreover, Figure 6 shows that the SERS signal of the linker is always present as weak features in the SERS spectrum. These features, however, may interfere with those from the species of interest. It is well known that both the position and the intensities of the SERS bands can be potential-dependent; hence, a detailed study of the SERS response of the substrate in the absence of a SERS probe is carried out.

In Situ SERS of the Substrates without a Probe Molecule

Figures 8 and 9 show the results of electrochemical stability tests in experiments without any SERS probe. The insets in

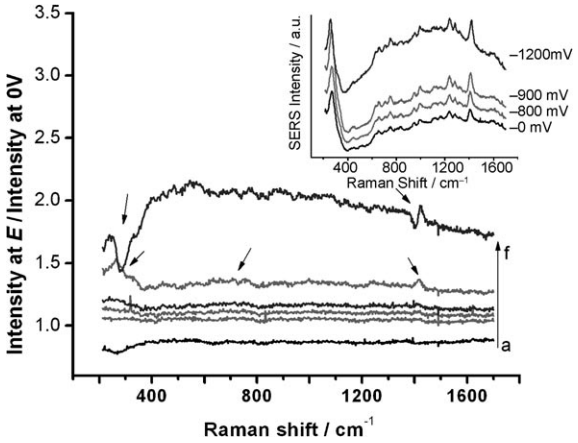

Figure 8. In situ SERS of the substrate. Applied potential from 0 to −1200 mV (vs. Ag/AgCl). Acquisition time, 180 s. Electrolyte, 0.1 M KCl. Ratio of the SERS spectrum at E = a) −200, b) −400, c) −600, d) −800, e) −900, and f) −1200 mV over that of E = 0 mV. The arrows indicate spectral changes. Inset: original spectra (raw data).

these figures present the raw SERS spectra of the substrate at different potentials; the background fluorescence and the vibrational bands of the PDT can be readily seen. Figure 8 corresponds to the SERS spectra obtained after the potential is stepped towards negative values from a starting potential of 0 V.

To better illustrate the changes in the SERS bands, all spectra are divided by the initial spectrum (0 V). This spectrum ratio is calculated for each potential using the raw SERS data (without baseline correction to eliminate the fluorescence), and the re-

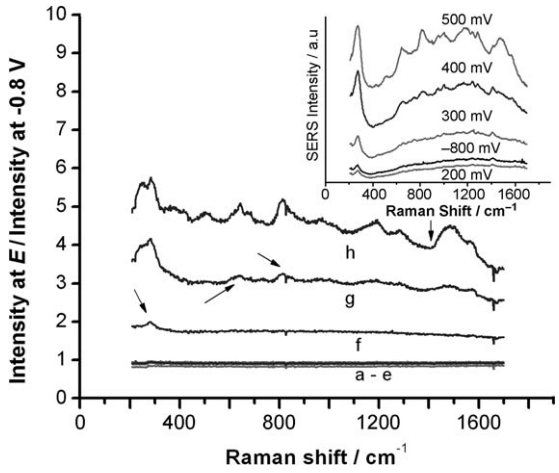

Figure 9. In situ SERS of the substrate. Applied potential from −800 to +500 mV (vs. Ag/AgCl). Acquisition time, 180 s. Electrolyte, 0.1 M KCl. Ratio of the SERS spectrum at E = a) −600, b) −400, c) −200, d) 0, e) +200, f) +300, g) +400, and h) +500 mV over that of E = −800 mV. The ratios (a) through (e) basically overlap. The arrows indicate spectral changes. Inset: original spectra (raw data).

sults are plotted in Figure 8. The ratios are close to one at all frequencies in the potential window between 0 and −800 mV, which indicates that no significant changes in peak position or intensity occur within that range. Even the fluorescence background did not change significantly. When the applied potential reaches −900 mV, a few changes, represented by arrows in Figure 8, are found in the electrochemical SERS spectra. New SERS bands growing at around 270, 600–700, and 1409 cm^{-1} are evident from the spectrum ratio at −900 mV and they are accompanied by an increase in the fluorescence background. These features (new vibrational bands and increased fluorescence background) become more evident as the potential is moved towards values more negative than −900 mV (Figure 8). The changes observed at −900 mV are attributed to the electroactivity of PDT at potentials more negative than −800 mV, since the desorption of alkanethiol from gold usually happens in the potential region between −800[55] and −1100 mV[56] versus Ag/AgCl. Therefore, we conclude that −800 mV is the limit in the negative range where the substrate is electrochemically inert and can be used for in situ SERS.

Similarly, in situ SERS tests were performed in the positive potential range. In this case, the starting potential was −800 mV and the normalized SERS spectra were calculated using the spectrum at this potential as reference. The raw spectra (inset) and the ratios can be found in Figure 9. The ratios are again constant in the potential range between −800 and +200 mV, but significant changes are observed after that positive potential limit. Note that after a full run beyond +200 mV, the original SERS signal decreases and cannot be recovered by stepping the potential back to values more negative than +200 mV. This finding indicates that irreversible structure changes take place after the limit of +200 mV.

The results from Figures 8 and 9 indicate that the substrate is not stable at potentials more negative than −800 mV and more positive than +200 mV. The SERS features of the background do not change significantly in the potential range between −800 and +200 mV. This implies that the substrates can be used for in situ SERS within that range, and that the potential-independent SERS signal from the interference (linker) could be subtracted.

In Situ SERS of the Substrates in the Presence of 4-HTP

Figure 10 presents the in situ SERS spectra of the probe molecule, 4-HTP, on an Au-NP-modified surface at different applied

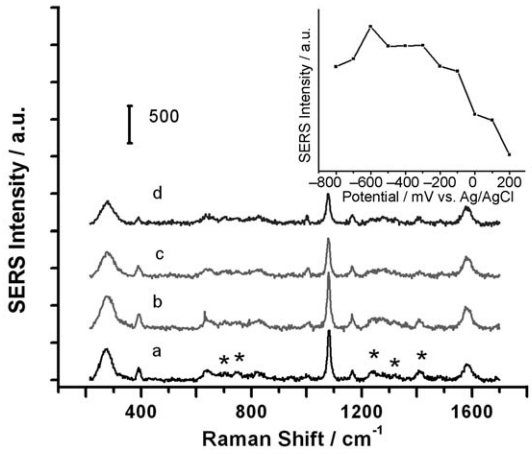

Figure 10. In situ SERS response of 4-HTTP: a) −800, b) −400, c) 0, and d) +200 mV versus Ag/AgCl. Electrolyte: 0.1 M KCl. The asterisks indicate the PDT bands (interference). Inset: change of SERS intensity of 4-HTP at 1080 cm^{-1} upon application of potential. The asterisks on spectrum a indicate the positions of some of the PDT bands.

potentials (within the potential range of the substrate stability determined in the previous section). The main features of 4-HTP can be readily identified at around 392, 636, 818, 1008, 1080, 1164, and 1584 cm^{-1}, which correspond to the 7a, 12, 6a, 18a, 1, 9a, and 8 (8a and 8b are mixed) modes, respectively, in terms of Wilson's notation.[49] Bands attributed to PDT are indicated by asterisks. The SERS signal from PDT is weak and provides a small interference. More importantly, the signal from PDT does not change with potential. The inset in Figure 10 shows a plot of the SERS intensity of the breathing mode of 4-HTP (1080 cm^{-1}) versus the applied potential. A maximum SERS signal is observed at around −600 mV. A decrease of the SERS signal at more negative potentials is expected because the desorption of 4-HTP will occur, as seen in cyclic voltammetric experiments involving thiols. The measurement of the electrochemical SERS trend of 4-HTP from the self-assembled substrate was possible. Hence, this substrate can be used in electrochemical SERS measurements, provided that the experiments are realized within the potential range of substrate stability and that the interferences from the PDT bands are recognized. The self-assembled substrates suggested here present better spatial and sample-to-sample reproducibility of the SERS spectra than the more conventional electrochemically roughened Au electrode. This is an important advantage of this substrate that could be further explored for the in situ in-

vestigation of electrocatalytic processes from nanostructured gold surfaces.

Conclusions

Three-dimensional nanostructured substrates were fabricated by the deposition of Au NPs on Au slides and used for surface-enhanced vibrational spectroscopy. The substrates were prepared by immersing the slide in a PDT solution, followed by incubation in a solution of Au NPs. This procedure was repeated until the desired number of Au-NP depositions was achieved. A substrate with only one Au-NP-deposition step provided the best enhancement for the probe molecule 4-HTP in surface-enhanced PM-IRRAS measurements. However, the linker PDT introduced some significant spectral interferences, thus reducing the applicability of this substrate in IR measurements. It was found that substrates made by 11 Au-NP depositions yielded the best SERS of 4-HTP for the 632.8 nm excitation. More importantly, substrates with more than nine Au-NP depositions presented a good spatial and batch-to-batch reproducibility (RSD lower than 20%). In situ SERS measurements showed that these substrates are stable in the potential window from -800 to $+200$ mV versus Ag/AgCl. In this region, SERS spectral interferences from the linker (PDT) did not change with the applied potential and were easily identified as weak features in the spectra. In situ SERS measurements of the probe molecule 4-HTP were obtained within the potential window of electrochemical stability of the substrate. The results discussed here also provide a baseline for further applications of this immobilization strategy in the fabrication of electrodes and substrates for high-sensitivity, SERS-based sensors.

Experimental Section

Chemicals: Unless otherwise mentioned, ACS-grade chemicals were used. The compounds $HAuCl_4$, sodium citrate dihydrate, PDT, and 4-HTP were obtained from Sigma–Aldrich. HPLC-grade methanol was obtained from Caledon Laboratories Ltd. Gold slides (100 nm-thick Au deposited on glass—a 5 nm Cr layer was used to help the adhesion of the gold to the glass) were obtained from Evaporated Metal Films Inc. Ultrapure water with a resistivity of 18.2 Ω cm (from Barnstead NANOpure Diamond water purification system) was used throughout the experiments.

Nanoparticle Synthesis: The glassware was cleaned by soaking overnight in a bath of hot sulfuric acid. After that, it was rinsed thoroughly with ultrapure water. The synthesis of Au NPs is described in the literature.[57] Briefly, $HAuCl_4$ solution (1 mM, 500 mL) was brought to a rolling boil with stirring. Sodium citrate solution (38.8 mM, 50 mL) was added and the heating and stirring were continued for 10 min. Then the heating was stopped and the stirring was continued for an additional 15 min to finish the reaction. The product solution was a wine-red color. The as-prepared Au NP solution was stored in an amber bottle in a fridge at 4 °C.

Gold-NP Deposition: Commercial Au slides were cleaned in an oxygen plasma for 15 min and then rinsed with methanol. The procedure for NP deposition, represented in Scheme 1, was as follows. Firstly, a gold slide was soaked in a methanolic solution of PDT (5 mM) for 24 h. A SAM of PDT was spontaneously formed on the gold surface. The slide modified with the PDT SAM was removed, rinsed with excess amounts of methanol and water, and incubated in a solution of Au NPs for another 24 h. After that, the slide with a monolayer of Au NPs was removed from the solution, dried with N_2, and rinsed with water. Subsequent Au NP depositions were accomplished by repeating the following steps: rinsing the slide carrying immobilized NPs with methanol and immersing it in PDT solution (5 mM) for 15 min to allow the PDT to self-assemble on the Au NP surface. The substrate was then rinsed with methanol and water and immersed in a solution of Au NPs for 1 h to deposit the Au NPs. The slide was dried with N_2 and rinsed with copious amounts of water. All samples were stored in water if not used immediately.

Application of the Probe Molecule 4-HTP: 4-HTP-coated slides were prepared by immersing the SERS substrates in an ethanolic solution of 4-HTP (1 mM) for 24 h. The samples were then rinsed with copious amounts of ethanol and dried with N_2.

Characterization: AFM was accomplished by using a ThermoMicroscopes digital AFM instrument, operated under ambient conditions in the noncontact mode. Noncontact AFM tips were obtained from ThermoMicroscopes (model 1650-00). An area of 1000×1000 nm^2 was always scanned (200 lines in the scan area) at a scan rate of 950 nm s^{-1}. Other parameters were optimized for each scan. UV/Vis reflection–absorption spectra of the as-prepared slides modified with Au NPs were measured by using a USB miniature fiber-optic spectrometer (Ocean Optics) attached to the ocular of an Olympus BHSM microscope. The halogen lamp of the microscope was used as light source. The experiments were realized in back-reflection mode using a 20× microscope objective.

PM-IRRAS: Measurements were performed on an Equinox 55 spectrometer (Bruker) equipped with a photoelastic modulator (PEM-90 with II/ZS50 ZnSe 50 kHz optical head, Hinds Instruments) and a liquid-N_2-cooled mercury cadmium telluride (MCT) IR detector (Kolmar Technologies). An external reflection configuration was used. The IR beam was directed to the sample surface at a grazing angle. The acquisition time was 10 min for the difference spectra and 2 min for the sum spectra. The resolution was set at 4 cm^{-1}. The final spectra were obtained by dividing the difference spectra by the sum spectra. The data presented were background subtracted.

Ex Situ and In Situ SERS: All the Raman measurements were accomplished by using a Raman microscope system equipped with an He–Ne laser source (632.8 nm, Melles Griot). Ex situ measurements were taken in air with the samples directly mounted on the stage of the Olympus BHSM microscope. The in situ measurements were taken with the substrate immersed in an electrolyte and under electrochemical control. The spectroelectrochemical cell used for in situ measurements was mounted on the stage of the microscope. The Raman experiments were realized in a backscattering configuration, where the exciting laser and the scattered radiation passed through the same 50× Olympus microscope objective. An ultralong-working-distance objective (NA = 0.55) was used for in situ measurements and a regular objective (NA = 0.80) was used for the ex situ measurements. A Kaiser super-notch filter was used to remove the unwanted radiation at the laser frequency. A Kaiser Holospec f/1.4 spectrograph equipped with an Andor CCD detector (model DV-401-BV) was coupled to the microscope. For in situ measurements, a three-compartment spectroelectrochemical cell with 1-mm glass window was used. The slides modified with Au NPs were used as working electrodes. An Ag/AgCl electrode was used as reference electrode and a Pt wire as counter elec-

trode. Typically, 30 s of acquisition time was applied for ex situ measurements while 120 s was used for in situ SERS. An Autolab PGSTAT 30 potentiostat/galvanostat was used to control the applied potential.

Acknowledgements

This research was funded by NSERC and Angstrom Power. An equipment grant was provided by the Canada Foundation for Innovation (CFI), the British Columbia Knowledge and Development Fund (BCKDF), and the University of Victoria through the New Opportunities Program.

Keywords: gold · nanoparticles · nanostructures · Raman spectroscopy · vibrational spectroscopy

[1] T. Vo-Dinh, *TrAC Trends Anal. Chem.* **1998**, *17*, 557–582.
[2] R. Aroca, *Surface-Enhanced Vibrational Spectroscopy*, Wiley, Hoboken, NJ, **2006**.
[3] S. M. Nie, S. R. Emery, *Science* **1997**, *275*, 1102–1106.
[4] G. A. Baker, D. S. Moore, *Anal. Bioanal. Chem.* **2005**, *382*, 1751–1770.
[5] A. G. Brolo, D. E. Irish, B. D. Smith, *J. Mol. Struct.* **1997**, *405*, 29–44.
[6] M. Osawa in *Surface-Enhanced Infrared Absorption, Vol. 81*, Springer, Berlin, **2001**, pp. 163–187.
[7] M. Osawa, *Bull. Chem. Soc. Jpn.* **1997**, *70*, 2861–2880.
[8] A. Campion, P. Kambhampati, *Chem. Soc. Rev.* **1998**, *27*, 241–250.
[9] K. W. Kho, Z. X. Shen, H. C. Zeng, K. C. Soo, M. Olivo, *Anal. Chem.* **2005**, *77*, 7462–7471.
[10] P. A. Mosier-Boss, S. H. Lieberman, *Anal. Chem.* **2005**, *77*, 1031–1037.
[11] L. G. Olson, R. H. Uibel, J. M. Harris, *Appl. Spectrosc.* **2004**, *58*, 1394–1400.
[12] H. G. Li, B. M. Cullum, *Appl. Spectrosc.* **2005**, *59*, 410–417.
[13] X. G. Hu, W. L. Cheng, T. Wang, Y. L. Wang, E. K. Wang, S. J. Dong, *J. Phys. Chem. B* **2005**, *109*, 19385–19389.
[14] R. Gomez, J. M. Perez, J. Solla-Gullon, V. Montiel, A. Aldaz, *J. Phys. Chem. B* **2004**, *108*, 9943–9949.
[15] R. G. Freeman, K. C. Grabar, K. J. Allison, R. M. Bright, J. A. Davis, A. P. Guthrie, M. B. Hommer, M. A. Jackson, P. C. Smith, D. G. Walter, M. J. Natan, *Science* **1995**, *267*, 1629–1632.
[16] L. L. Bao, S. M. Mahurin, S. Dai, *Anal. Chem.* **2004**, *76*, 4531–4536.
[17] R. F. Aroca, P. J. G. Goulet, D. S. dos Santos, R. A. Alvarez-Puebla, O. N. Oliveira, *Anal. Chem.* **2005**, *77*, 378–382.
[18] R. F. Aroca, R. A. Alvarez-Puebla, N. Pieczonka, S. Sanchez-Cortez, J. V. Garcia-Ramos, *Adv. Colloid Interface Sci.* **2005**, *116*, 45–61.
[19] S. P. Mulvaney, C. D. Keating, *Anal. Chem.* **2000**, *72*, 145R–157R.
[20] C. L. Leverette, S. A. Jacobs, S. Shanmukh, S. B. Chaney, R. A. Dluhy, Y.-P. Zhao, *Appl. Spectrosc.* **2006**, *60*, 906–913.
[21] J. V. Coe, S. M. Williams, K. R. Rodriguez, S. Teeters-Kennedy, A. Sudnitsyn, F. Hrovat, *Anal. Chem.* **2006**, *78*, 1384–1390.
[22] S.- J. Huo, X.- K. Xue, Q.-X. Li, S.-F. Xu, W.-B. Cai, *J. Phys. Chem. B* **2006**, *110*, 25721–25728.
[23] S. J. Huo, Q. X. Li, Y. G. Yan, Y. Chen, W. B. Cai, Q. J. Xu, M. Osawa, *J. Phys. Chem. B* **2005**, *109*, 15985–15991.
[24] D. Enders, A. Pucci, *Appl. Phys. Lett.* **2006**, *88*, 184104.
[25] C. W. Brown, Y. Li, J. A. Seelenbinder, P. Pivarnik, A. G. Rand, S. V. Letcher, O. J. Gregory, M. J. Platek, *Anal. Chem.* **1998**, *70*, 2991–2996.
[26] D. Enders, S. Rupp, A. Kuller, A. Pucci, *Surf. Sci.* **2006**, *600*, L305–L308.
[27] A. Miki, S. Ye, M. Osawa, *Chem. Commun.* **2002**, 1500–1501.
[28] M. D. Musick, C. D. Keating, M. H. Keefe, M. J. Natan, *Chem. Mater.* **1997**, *9*, 1499–1501.
[29] C. J. Addison, A. G. Brolo, *Langmuir* **2006**, *22*, 8696–8702.
[30] I. W. Sztainbuch, *J. Chem. Phys.* **2006**, *125*, 124707.
[31] L. G. Olson, Y. S. Lo, T. P. Beebe, J. M. Harris, *Anal. Chem.* **2001**, *73*, 4268–4276.
[32] A. I. Abdelrahman, A. M. Mohammad, T. Okajima, T. Ohsaka, *J. Phys. Chem. B* **2006**, *110*, 2798–2803.
[33] M. D. Musick, D. J. Pena, S. L. Botsko, T. M. McEvoy, J. N. Richardson, M. J. Natan, *Langmuir* **1999**, *15*, 844–850.
[34] M. D. Musick, C. D. Keating, L. A. Lyon, S. L. Botsko, D. J. Pena, W. D. Holliway, T. M. McEvoy, J. N. Richardson, M. J. Natan, *Chem. Mater.* **2000**, *12*, 2869–2881.
[35] C. W. Welch, R. G. Compton, *Anal. Bioanal. Chem.* **2006**, *384*, 601–619.
[36] D. Hernandez-Santos, M. B. Gonzalez-Garcia, A. C. Garcia, *Electroanalysis* **2002**, *14*, 1225–1235.
[37] M. C. Daniel, D. Astruc, *Chem. Rev.* **2004**, *104*, 293–346.
[38] R. Gómez, J. Solla-Gullón, J. M. Pérez, A. Aldaz, *J. Raman Spectrosc.* **2005**, *36*, 613–622.
[39] X.-Y. Li, Q.- J. Huang, V. I. Petrov, Y.-T. Xie, Q. Luo, X. Yu, Y.- J. Yan, *J. Raman Spectrosc.* **2005**, *36*, 555–573.
[40] L. Guo, Q. J. Huang, X. Y. Li, S. H. Yang, *Phys. Chem. Chem. Phys.* **2001**, *3*, 1661–1665.
[41] J. N. Som, D. K. Mukherjee, *J. Mol. Struct.* **1975**, *26*, 120–123.
[42] S. W. Joo, S. W. Han, K. Kim, *J. Phys. Chem. B* **2000**, *104*, 6218–6224.
[43] S. Bernad, W. Mantele, *Anal. Biochem.* **2006**, *351*, 214–218.
[44] J. A. Seelenbinder, C. W. Brown, P. Pivarnik, A. G. Rand, *Anal. Chem.* **1999**, *71*, 1963–1966.
[45] E. Bahar, G. R. Huang, B. S. Lee, *Radio Sci.* **1995**, *30*, 525–544.
[46] D. Bicout, C. Brosseau, A. S. Martinez, J. M. Schmitt, *Phys. Rev. E* **1994**, *49*, 1767–1770.
[47] A. Sivanesan, P. Kannan, S. A. John, *Electrochim. Acta* **2007**, *52*, 8118–8124.
[48] T. Itoh, V. Biju, M. Ishikawa, Y. Kikkawa, K. Hashimoto, A. Ikehata, Y. Ozaki, *J. Chem. Phys.* **2006**, *124*, 134708.
[49] H. M. Lee, M. S. Kim, K. Kim, *Vib. Spectrosc.* **1994**, *6*, 205–214.
[50] C. J. Addison, MSc Thesis, University of Victoria (Canada), **2005**.
[51] E. Tourwe, A. Hubin, *Vibr. Spectrosc.* **2006**, *41*, 59–67.
[52] S. Yun, Y. K. Park, S. K. Kim, S. Park, *Anal. Chem.* **2007**, *79*, 8584–8589.
[53] L. D. Qin, S. L. Zou, C. Xue, A. Atkinson, G. C. Schatz, C. A. Mirkin, *Proc. Natl. Acad. Sci. USA* **2006**, *103*, 13300–13303.
[54] F. Le, N. Z. Lwin, J. M. Steele, M. Kall, N. J. Halas, P. Nordlander, *Nano Lett.* **2005**, *5*, 2009–2013.
[55] H. Wano, K. Uosaki, *Langmuir* **2005**, *21*, 4024–4033.
[56] M. M. Walczak, D. D. Popenoe, R. S. Deinhammer, B. D. Lamp, C. K. Chung, M. D. Porter, *Langmuir* **1991**, *7*, 2687–2693.
[57] K. C. Grabar, R. G. Freeman, M. B. Hommer, M. J. Natan, *Anal. Chem.* **1995**, *67*, 735–743.

Received: February 19, 2008
Revised: May 5, 2008
Published online on August 14, 2008

